2012 Workshop on Engine and Powertrain Control, Simulation and Modeling
The International Federation of Automatic Control
Rueil-Malmaison, France, October 23-25, 2012

Evaluating the Potential for Cell Balancing Using a Cascaded Multi-Level Converter Using Convex Optimization ⋆

Faisal Altaf * **Lars Johannesson** ** **Bo Egardt** ***

* *e-mail: faisal.altaf@ chalmers.se*
** *e-mail: larsjo@ chalmers.se*
*** *e-mail: bo.egardt@ chalmers.se.*
Chalmers University of Technology, Göteborg, Sweden

Abstract: The modeling and design of an active battery cell balancing system using Multi-Level Converter (MLC) for EV/HEV/PHEV is studied. The MLC allows to independently switch ON/OFF each battery cell in a battery pack . This extra degree-of-freedom (DoF) can be exploited to optimally use each cell in order to balance among them the temperature and state-of-charge (SoC). This study has shown that the constrained convex optimization based control policy, exploiting the extra DoF of MLC, gives significant benefit in terms of reduction in temperature and SoC deviations, especially under parameter variations, compared to uniformly using all the cells. Thus, the MLC has promising potential to offer extra benefit of achieving cell balancing while being simultaneously used as a motor driver.

Keywords: Hybrid Vehicles, Multi-level Converter, Cell Balancing, Convex Optimization.

1. INTRODUCTION

Driven by the needs to reduce the dependence of fossil fuels and the environmental impact of transportation there has in recent years been an increasing interest in the electrification of vehicles. The still relatively low specific energy and the high cost of available battery technology means that Hybrid Electric Vehicles (HEVs) and Plug-in Hybrid Electric Vehicles (PHEVs) are in the short term horizon more likely to reach a wide spread impact on the market than pure Electric Vehicles (EVs). Common to both (P)HEVs and EVs is that the battery is one of the most expensive components in the powertrain, contributing largely to the total vehicle cost. As a result, the battery lifetime is an important factor for the success of (P)HEVs and EVs.

The battery pack (BP) is built from large number of small cells connected in series and parallel to meet both the traction power demand and electric range requirement. The Depth-of-Discharge (DoD) is one of the most important factors that determines the degradation of the battery cells, see Kuhn et al. (2005), Lukic et al. (2008), and Smith et al. (2010). To ensure uniform life-time of the cells it is therefore important to utilize each cell so that the State-of-Charge (SoC) and respectively the DoD, remains almost balanced in all cells of the battery pack. Another factor that strongly influences the lifetime is the cell temperature; hotter cells degrade more quickly than colder cells, see Park and Jaura (2003b), Park and Jaura (2003a), Park and Jaura (2002), and Pesaran and Vlahinos (1997). Therefore, even a few overheated cells may result in shortening the lifetime of the whole battery pack. Temperature imbalance between cells is mainly caused by variation in internal resistances, temperature gradient in coolant due to convective heat transfer alongside the battery pack, and non-uniform external local thermal disturbances, see Pesaran and Vlahinos (1997) and Mahamud and Park (2011). It has been reported that the lifetime of Li-Ion cell is reduced by two months for each degree of temperature rise in an operating temperature range of 30 to 40°C, see Motloch et al. (2002), and above 40°C it decreases drastically.

Hence, the Battery Management Unit (BMU) should ideally be able to both balance the SoC of the cells and keep the temperature differences between the cells less than 5°C with a maximum temperature below 40°C, see Park and Jaura (2003a). Forced convection cooling is normally used to keep the batteries within recommended operating temperature range but suffers from temperature gradient problem due to convective heat transfer along the coolant fluid stream. The reciprocating air-flow has been proposed by Park and Jaura (2003b) and Mahamud and Park (2011) to improve temperature uniformity in the battery system, but in the presence of parameter variation and local disturbances cells can still suffer from non-uniform local heated spots. In addition to forced cooling of the battery system, there are several active and passive cell balancing schemes. These are based on various topologies of switched capacitive and resistive circuits, see for example Lee et al. (2011),Cao et al. (2008), Bentley (1997), and Krein (2007). The main idea behind all active balancing schemes is to transfer the charge from cells having higher SoC to cells having lower SoC through switched capacitors which act as intermediate storage banks.

In recent years cascaded multi-level converters, see Rodriguez et al. (2009) and Malinowski et al. (2010), have

⋆ The work of the authors was supported by the Chalmers Energy Initiative.

been thoroughly investigated and discussed for the drive of electric motor in HEVs, see Tolbert et al. (1999) and Josefsson et al. (2010). The MLC consists of n cascaded H-bridges with an isolated battery cell for each H-bridge. The combination of an H-bridge and a battery cell is called a Power Cell (PC). The MLC, other than reducing total harmonic distortion (THD) in generated waveform for electric machine, also offers an additional advantage of extra degree of freedom to generate the load voltages.

In most of these motor drive applications of MLCs, the usual strategy is to use Phase Shifted Pulse Width Modulation (PS-PWM) technique to achieve uniform use of cascaded cells, see Rodriguez et al. (2009) and Malinowski et al. (2010). However, since the cells are not identical and operate in different conditions, SoC and thermal imbalance cannot be avoided. Here the PS-PWM scheme is denoted as `UDCO` (Uniform Duty Cycle Operation).

The main contribution of this article is to investigate the potential benefit of using the MLC to balance both the SoC and the temperature among the battery cells. The optimal control policy is calculated in a convex optimization problem based on the assumption of perfect information of the SoC and temperature of each cell as well as of the future driving. In this article, the optimal policy is called `OP` (Optimal Policy). The main research task is to investigate if `OP` gives a significant benefit compared to `UDCO` . At this initial stage, it is evaluated through simulations. For simplicity, in this early study the electric machine is assumed to be a DC machine and the cells are modeled by resistive circuits. Moreover, the simulation study is focused only on an air-cooled battery sub-module (`BSM`) with 5 series-connected cells. The coolant flow is assumed to be laminar with known inlet temperature and speed. The resistance of the thermally exposed downstream cell is varied to carefully examine the performance of the `UDCO` and `OP` . Another important contribution of this article is the detailed derivation of a state-space electro-thermal model of a battery submodule under the switching action of an MLC. The model is formulated in the context of battery management and optimization. It is pertinent to mention here that though, for the sake of completion, the model with three electrical states of a battery cell have been derived but inside the optimization, some assumptions are made to simplify the problem.

The paper is organized as follows. Section 2 gives an overview of basic function of MLC. The detailed electro-thermal modeling of battery sub-module under the switching action of MLC is given in Section 3. Section 4 defines the optimization problem and discusses the numerical solution method. The simulation results and comparison between `OP` and `UDCO` scheme is given in Section 5 and conclusion and future work are highlighted in Section 6.

2. MULTI-LEVEL CONVERTERS OVERVIEW

In contrast to two voltage-level converters, consisting of a single large battery connected with a single H-bridge (HB), the MLC consists of many series connected Power Cells (PC) where each PC contains an H-bridge and the independent battery cell as shown in Figure 1. The H-bridge is a switch mode dc-dc power converter, see Mohan et al. (2003), that produces a four-quadrant

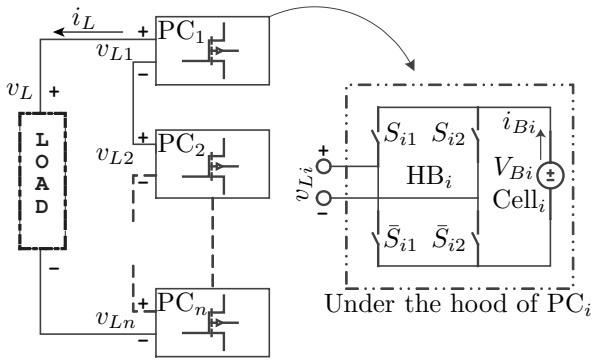

Fig. 1. Block diagram of a single phase cascaded H-bridge multi-level converter. To avoid the shoot-through problem only one of the switch pairs $(S_{i1}\,,\bar{S}_{i2})$, $(S_{i2}\,,\bar{S}_{i1})$,$(S_{i1}\,,S_{i2})$ or $(\bar{S}_{i1}\,,\bar{S}_{i2})$ is allowed to turn-on at a time. The pair $(S_{i1}\,,\bar{S}_{i2})$ generates positive v_{Li} and $(S_{i2}\,,\bar{S}_{i1})$ gives negative v_{Li} whereas both switch pairs $(S_{i1}\,,S_{i2})$ and $(\bar{S}_{i1}\,,\bar{S}_{i2})$ gives $v_{Li}=0$.

controllable dc output using four switches $S_{i1}\,,S_{i2}\,,\bar{S}_{i1},\bar{S}_{i2}$ as shown in Figure 1. Therefore, depending on which switch pair is turned-on, three modes of operation can be defined for each PC_i. In *Mode–1* $v_{Li}>0$, in *Mode–2* $v_{Li}<0$ and in *Mode–3* $v_{Li}=0$. To model these three modes of operation, let's define $S_{ij}=1$ for ON-State and $S_{ij}=0$ for OFF-State of switch S_{ij} where 'i' corresponds to PC_i and $j\in\{1,2\}$. Now the switching function $s_i(t)$ for a Cell_i can be defined by $s_i(t)=(S_{i1}-S_{i2})\in\{1,-1,0\}$ corresponding to *Mode–1*, *Mode–2* and *Mode–3* respectively. The switching vector $s(t)=[s_1(t)\;s_2(t)\;\cdots\;s_n(t)]^T$ contains switching functions for all n PCs inside the MLC. Thus all three modes of H-bridge can be defined in terms of $s_i(t)$. Assuming the ideal switch behavior, the ohmic and switching losses can be ignored and, therefore, the input and output of H-bridge, as shown in Figure 1, are related through the switching function $s_i(t)$. Thus, the current through Cell_i is given by:

$$i_{Bi}(t)=i_L(t)s_i(t) \tag{1}$$

Note that due to the series connection, the same current i_L pass through each PC. However, the direction of current passing through the battery Cell_i depends both on the selection of switches and the direction of load current i_L. Similarly the voltage output from each PC_i is defined by $v_{Li}(t)=V_{Bi}(t)s_i(t)$ and hence the total voltage output from the MLC can be written as the sum of voltage output from each PC_i

$$v_L=\sum_{i=1}^{n}v_{Li}=\sum_{i=1}^{n}V_{Bi}(t)\,s_i(t) \tag{2}$$

with the MLC being able to generate $L=2\,n+1$ different voltage levels (v_L).

3. MODELING OF CELL BALANCING SYSTEM

The block diagram of the cell balancing system is shown in Figure 2. In this section, based on the assumption that the load is a DC-machine, first the switching model and then the averaged-state-space model of a power cell is derived and finally the complete state-space model for n power cells is given.

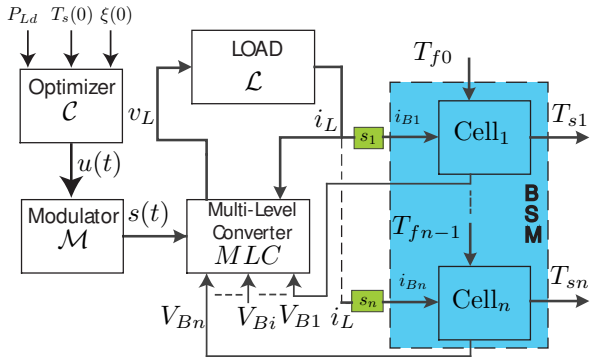

Fig. 2. Conceptual block diagram of battery cell balancing system. $T_s(0)$ is a vector containing initial temperature of all cells and $\xi(0)$ is a vector containing initial SoC of all cells, P_{Ld} is the demanded power for load with the known voltage and current profile and $T_{f0}, \cdots, T_{fn-1}$ represent coolant fluid temperature-nodes. The subsystem inside blue box is a battery submodule (BSM) being balanced and green boxes contain switching functions for the corresponding cell.

3.1 Switching Model of a Power Cell

In this subsection, the electro-thermal model of a switched battery cell is derived. The dynamics of cell temperature depends on many factors like coolant properties, cell material properties, cell placement and battery pack configuration. The forced-convection cooled battery pack has been modeled using *Lumped-capacitance Thermal Model* and *Flow Network Model* (FNM) by Mahamud and Park (2011). In their study, the battery pack is configured as $n_s S n_p P$ which means n_p parallel strings (each string is called battery module) with each string having n_s cells connected in series. There is a sufficient free space between cells to allow streams of laminar flow of coolant (air). In this paper, the configuration of battery pack used is similar to that of Mahamud and Park (2011) with similar Li-Ion cells and air properties. The various coefficients for thermal and physical properties of cell and air used in this study are given in Table 1, see Mahamud and Park (2011) for details. The $C_{Ni}\,[Ah]$ is the nominal capacity of battery Cell$_i$ and

Table 1. Definition of Battery Parameters

Parameters	Expression	Parameters	Expression
$a_{si}\ [\frac{1}{s}]$	$\left(\frac{1}{C_{si}R_{ui}}\right)$	$b_{ri}\ [\Omega]$	R_{si}
$a_{ei1}\ [\frac{1}{s}]$	$\left(\frac{1}{R_{i1}C_{i1}}\right)$	α_i [Unitless]	$R_{ui}\mathrm{c_f}$
$a_{ei2}\ [\frac{1}{s}]$	$\left(\frac{1}{R_{i2}C_{i2}}\right)$	β_i [Unitless]	$-1+\alpha_i$
$b_{si}\ [\frac{\Omega K}{W s}]$	$\left(\frac{R_{si}}{C_{si}}\right)$	$b_{ei2}\ [\frac{V}{s A}]$	$\left(\frac{1}{C_{i2}}\right)$
$b_{ei1}\ [\frac{V}{s A}]$	$\left(\frac{1}{C_{i1}}\right)$	$b_{ei3}\ [\frac{1}{A s}]$	$\left(\frac{1}{3600C_{Ni}}\right)$

$R_{ui}\,[KW^{-1}]$ is the convection thermal resistance for Cell$_i$ and its value depends upon the geometry of the battery cell, coolant fluid properties and Nusselt number which in turn depends on Reynolds number. The coefficient $C_{si} = \rho_{si} c_{psi} V_{si}\,[JK^{-1}]$ is the *Heat Capacity* whereas ρ_{si} is the density, c_{psi} is the *Specific Heat Capacity* and $V_{si}\,[m^3]$ is the volume of Cell$_i$. The coefficient $\mathrm{c_f} = \rho_f c_{pf} \dot{V}_f\,[WK^{-1}]$ is the *Thermal Conductance* of the coolant fluid. All other quantities are shown in Figure 3.

In this paper, only one submodule (of a battery module), that consists of n series connected battery cells, is studied. The thermal model proposed by Mahamud and Park (2011) does not consider any power electronic switching of battery cells, so it must be adapted to the current framework. Thus, it is modified by embedding the switching function $s_i(t)$ and then it is combined with the enhanced Thevenin equivalent electrical model shown in Figure 3 to derive the switching electro-thermal model of a PC$_i$ as follows. Assuming that the coolant flow direction is from lower to higher cell index, the dynamics of the surface temperature $T_{si}\,[K]$ of the battery Cell$_i$ in terms of $i_L(t)$ and $s_i(t)$, after substituting the value of $i_{Bi}(t)$ from (1) into the model proposed by Mahamud and Park (2011), is given by:

$$\dot{T}_{si} = -a_{si} T_{si} + b_{si} i_L^2 s_i^2 + a_{si} T_{fi-1}, \quad \forall i = \{1, \cdots, n\} \tag{3}$$

where the term $i_L^2 s_i^2$ represents the instantaneous ohmic power losses on the Cell$_i$ and $T_{fi-1}\,[K]$ is the temperature of temperature–node '$i-1$' (of fluid element modeled using FNM) attached to Cell$_i$ in upstream direction. According to Mahamud and Park (2011), the temperatures of temperature–node '$i-1$' and 'i' are related by:

$$T_{fi} = \frac{(T_{si} + \beta_i\, T_{fi-1})}{\alpha_i}, \forall i \tag{4}$$

By a forward recursion of equation (4), any T_{fi} can be expressed as a function of inlet fluid temperature T_{f0} and the temperatures T_{s1} to T_{si} of battery cells. Thus:

$$T_{fi} = a_{fi1}\, T_{s1} + a_{fi2}\, T_{s2} + \cdots + a_{fii}\, T_{si} + b_{fi}\, T_{f0} \tag{5}$$

where:

$$a_{fii} = \left(\frac{1}{\alpha_i}\right), \quad b_{fi} = \left(\frac{\prod_{k=1}^{i} \beta_k}{\prod_{k=1}^{i} \alpha_k}\right), \quad \forall i \geq 1 \tag{6}$$

$$a_{fij} = \left(\frac{\prod_{k=(j+1)}^{i} \beta_k}{\prod_{k=j}^{i} \alpha_k}\right), \quad \forall i > j, \quad a_{fij} = 0, \quad \forall i < j \tag{7}$$

Now using the expression (5) in (3), the thermal dynamics of battery cells can be re-written as follows:

$$\dot{T}_{si} = a_{ti1}\, T_{s1} + \cdots + a_{tii}\, T_{si} + b_{si}\, i_L^2\, s_i^2 + b_{ti}\, T_{f0} \tag{8}$$

where:

$$a_{tii} = -a_{si}, \quad \forall i \geq 1 \tag{9}$$

$$a_{tij} = \left(\frac{\prod_{k=(j+1)}^{(i-1)} \beta_k}{\prod_{k=j}^{(i-1)} \alpha_k}\right) a_{si}, \quad \forall i > j, \quad a_{tij} = 0, \quad \forall i < j \tag{10}$$

$$b_{ti} = \left(\frac{\prod_{k=1}^{(i-1)} \beta_k}{\prod_{k=1}^{(i-1)} \alpha_k}\right) a_{si}, \quad \forall i \geq 1 \tag{11}$$

The electrical equivalent model of a battery cell is shown in Figure 3. It is an enhanced Thevenin Model with two time constant behavior, see Codeca et al. (2008), Chen and Rincon-Mora (2006), He et al. (2011). The dynamic model for this circuit is given by

$$\dot{V}_{i1} = -a_{ei1} V_{i1} + b_{ei1} i_L s_i, \tag{12}$$

$$\dot{V}_{i2} = -a_{ei2} V_{i2} + b_{ei2} i_L s_i, \tag{13}$$

$$\dot{\xi}_i = -b_{ei3} i_L s_i, \tag{14}$$

$$V_{Bi} = f(\xi_i) - V_{i1} - V_{i2} - b_{ri} i_L s_i \tag{15}$$

where i_{Bi} is the current flowing through the Cell$_i$ and ξ_i is the normalized state-of-charge (SoC) of Cell$_i$. Note that

$\xi_i \in [0,1]$ is a unit-less quantity. The V_{i1} and V_{i2} are the voltages across capacitors C_{i1} and C_{i2} respectively and V_{Bi} is the output voltage of Cell$_i$. The SoC dependent open circuit voltage is given by $V_{oci} = f(\xi_i)$ where $f : [0,1] \to \mathbb{R}_0^+$ is a function of SoC. Note that equations (8)–(15) describe the switched behavior of battery, under the switching action of the MLC, in terms of load current $i_L(t)$ and the switching function $s_i(t)$ and therefore we call it a *switching model* of a power cell PC$_i$.

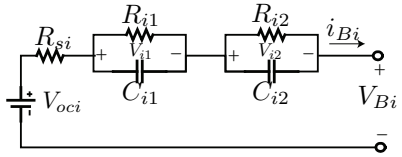

Fig. 3. Electrical model of a battery cell.

3.2 Averaged-State-Space Model of a Power Cell

In this study the aim is to evaluate the OP and for that a model with real-valued control signal, which is far easier to handle in optimization problem compared to the case of discrete-valued signals, is needed. Since the switching model (8)–(15) involves discrete-valued signals $s_i(t)$, it is required to transform these signals to real-valued, averaged signals and modify the system model accordingly. The justification for use of averaging comes from the fact that, in most cases, the switching frequency F_s inside the modulator $\mathcal{M}$ is much higher than the bandwidth f_L of the system. So under the assumption $F_s \gg f_L$ and employing the two-time scale separation principle, see Khalil (2002), the concept of averaging can be employed, see Sirisukprasert (2004) and Kassakian et al. (1991). In other words it is assumed that the system response is determined predominantly by the duty cycle $u_i(t) \in [-1,1]$ i.e. the average of the switching input function $s_i(t)$. The following assumptions are made for derivation of the average quantities:

Assumption 1. The switching function can only attain values either from the set $\{0,1\}$ or $\{0,-1\}$ during any switching cycle of period T_s. This assumption implies that it is not allowed to charge and discharge the battery cell during the same switching cycle.

Assumption 2. The load current $i_L(t)$ remains fairly constant during any switching cycle. This assumption is justified based on the discussion above.

Assumption 3. All the internal electrical states $V_{i1} = \bar{V}_{i1}$, $V_{i2} = \bar{V}_{i2}$ and $\xi_i = \bar{\xi}_i$ and the terminal voltage V_{Bi} remains fairly constant during the switching cycle. Thus, the battery output voltage can now be rewritten as follows:

$$V_{Bi} = f(\bar{\xi}_i) - \bar{V}_{i1} - \bar{V}_{i2} - b_{ri} i_{Bi} \tag{16}$$

Based on these assumptions, the average of the switching function $s_i(t)$ which is also called the duty-cycle is given by:

$$u_i(t) = \bar{s}_i(t) = \frac{1}{T_s}\int_{t-T_s}^{t} s_i(t)\mathrm{d}t \tag{17}$$

Defining $T_{on} \in [0, T_s]$ as the time duration for which $s_i(t)$ is non-zero (i.e. ± 1) and $s_p \in \{-1, 1\}$ as the peak value of $s_i(t)$ and then using assumption 1, the expression for the duty cycle over the first switching cycle, $t \in [0, T_s]$, is given by:

$$u_i(t) = \frac{1}{T_s}\left(\int_0^{T_{on}} s_p\,\mathrm{d}t + \int_{T_{on}}^{T_s} 0\,\mathrm{d}t\right) = \pm\frac{T_{on}}{T_s} \tag{18}$$

Now it can be clearly seen from (18) that depending on the value of T_{on} and s_p, $u_i(t)$ can attain any continuous real value in the interval $[-1, 1]$. Also note that $u_i \in (0\,, 1]$ means switching between Mode–1 and Mode–3 and $u_i \in [-1\,, 0)$ means switching between Mode–2 and Mode–3 and $u_i = 0$ corresponds to Mode–3. An example of averaging of switching function is shown in Figure 4.

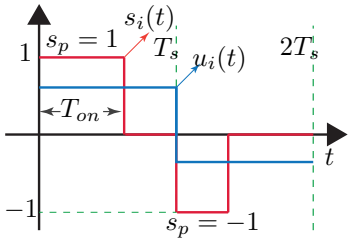

Fig. 4. Averaging of switching function $s_i(t)$.

Now all other averaged signals can be defined in terms of $u_i(t)$ and $i_L(t)$. The average current $\bar{i}_{Bi}$ flowing through Cell$_i$ during interval T_s is given by:

$$\bar{i}_{Bi}(t) = \frac{1}{T_s}\int_{t-T_s}^{t} i_{Bi}(t)\mathrm{d}t = u_i\, i_L \tag{19}$$

Similarly using assumption-3 and equation (16), the average terminal voltage of the battery cell is given by

$$\bar{V}_{Bi} = \frac{1}{T_s}\int_0^{T_s} V_{Bi}\mathrm{d}t = f(\bar{\xi}_i) - \bar{V}_{i1} - \bar{V}_{i2} - b_{ri} i_L u_i \tag{20}$$

which is now interpreted as the average voltage output of battery Cell$_i$ under the flow of average battery current $\bar{i}_{Bi}$. Similarly the average output voltage from PC$_i$ during period T_s of any switching cycle is given by:

$$\begin{aligned}\bar{v}_{Li} &= \frac{1}{T_s}\int_0^{T_s} v_{Li}\mathrm{d}t = \frac{1}{T_s}\int_0^{T_s} V_{Bi} s_i \mathrm{d}t \\ \bar{v}_{Li} &= f(\bar{\xi}_i)u_i - \bar{V}_{i1}u_i - \bar{V}_{i2}u_i \\ &\quad - \frac{b_{ri}\, i_L}{T_s}\left(\int_0^{|u_i|T_s} s_i^2\mathrm{d}t + \int_{|u_i|T_s}^{T_s} 0\,\mathrm{d}t\right)\end{aligned} \tag{21}$$

Since $s_i^2 = s_p^2 = 1$ during ON time, the above expression simplifies to:

$$\bar{v}_{Li} = \left(f(\bar{\xi}_i) - \bar{V}_{i1} - \bar{V}_{i2}\right) u_i - b_{ri}|u_i| i_L \tag{22}$$

and therefore the total output voltage from multi-level converter is given by:

$$\bar{v}_L = \sum_{i=1}^{n}\left[\left(f(\bar{\xi}_i) - \bar{V}_{i1} - \bar{V}_{i2}\right) u_i - b_{ri}|u_i| i_L\right] \tag{23}$$

Since the quadratic quantity $i_{Bi}^2(t)$ is responsible for heat generation inside the cell, we need to compute the corresponding average quantity which incurs the equivalent ohmic losses over one switching cycle. From the circuit analysis we know the root-mean-square (RMS) current i_{Br_i} is that effective dc current given by:

$$i_{Br_i}^2 = \frac{1}{T_s}\int_0^{T_s} i_{Bi}^2\mathrm{d}t = \frac{1}{T_s}\left(\int_0^{|u_i|T_s} s_i^2\, i_L^2\mathrm{d}t + \int_{|u_i|T_s}^{T_s} 0\,\mathrm{d}t\right)$$

and using the assumptions, the above expression simplifies to:

$$i^2_{Br_i} = |u_i| i^2_L = \left(\frac{T_{on}}{T_s}\right) i^2_L \tag{24}$$

Similarly the average power being delivered by the Cell_i during the switching period T_s is now given by:

$$P_i = \bar{v}_{Li} i_L = f(\bar{\xi}_i) u_i i_L - \bar{V}_{i1} u_i i_L - \bar{V}_{i2} u_i i_L - b_{ri} |u_i| i^2_L \tag{25}$$

Now using the averaged quantities (19),(24) the *averaged-model* of PC_i can be written as follows:

$$\dot{\bar{T}}_{si} = a_{ti1}\, \bar{T}_{s1} + \cdots + a_{tii}\, \bar{T}_{si} + b_{si}\, i^2_L\, |u_i| + b_{ti}\, T_{f0} \tag{26}$$

$$\dot{\bar{V}}_{i1} = -a_{ei1} \bar{V}_{i1} + b_{ei1} i_L u_i \tag{27}$$

$$\dot{\bar{V}}_{i2} = -a_{ei2} \bar{V}_{i2} + b_{ei2} i_L u_i \tag{28}$$

$$\dot{\bar{\xi}}_i = -b_{ei3} i_L u_i \tag{29}$$

$$\bar{V}_{Bi} = f(\bar{\xi}_i) - \bar{V}_{i1} - \bar{V}_{i2} - b_{ri} i_L u_i \tag{30}$$

Since $|u_i|$ in (26) is not continuously differentiable, we define u_i and $|u_i|$ in terms of two new control variables u_{i1} and u_{i2} which are defined as: $u_{i1} = \max\{0, u_i\} \in [0\,, 1]$ and $u_{i2} = \max\{0, -u_i\} \in [0\,, 1]$. Now we can write $u_i = (u_{i1} - u_{i2}) \in [-1\,, 1]$ and $|u_i| = (u_{i1} + u_{i2}) \in [0\,, 1]$. Note that u_{i1} can now be interpreted as duty cycle for Mode–1 whereas u_{i2} can be interpreted as duty cycle for Mode–2. In this new context, u_{i1} and u_{i2} can not be non-zero simultaneously (cf. assumption 1) at any time instant due to safety reasons which if violated can cause shoot-through. Thus in terms of newly defined control signal, the thermal subsystem of battery Cell_i, for coolant flow from lower to higher cell index, is given by:

$$\dot{X}_{ti} = a_{ti1}\, X_{t1} + \cdots + a_{tii}\, X_{ti} + \hat{g}_{ti}(x_L)\, \hat{u}_i + b_{ti} T_{f0} \tag{31}$$

where $X_{ti} = \bar{T}_{si} \in \mathbb{R}$, $\hat{g}_{ti}(x_L) = \begin{bmatrix} b_{si} x^2_L & b_{si} x^2_L \end{bmatrix}$, $\hat{u}_i = \begin{bmatrix} u_{i1} & u_{i2} \end{bmatrix}^T \in \mathbb{R}^2$ and $x_L = i_L$. Similarly, the electrical subsystem of battery Cell_i is given by:

$$\dot{X}_{ei} = A_{ei} X_{ei} + \hat{g}_{ei}(x_L)\, \hat{u}_i \tag{32}$$

where $X_{ei} = \begin{bmatrix} X_{ei1} & X_{ei2} & X_{ei3} \end{bmatrix}^T \in \mathbb{R}^3$ with $X_{ei1} = \bar{V}_{i1}$, $X_{ei2} = \bar{V}_{i2}$, $X_{ei3} = \bar{\xi}_i$ and $A_{ei} = \text{diag}\,(-a_{ei1}, -a_{ei2}, 0) \in \mathbb{R}^{3\times 3}$, $\hat{g}_{ei}(x_L) = \begin{bmatrix} b_{ei} x_L & -b_{ei} x_L \end{bmatrix} \in \mathbb{R}^{3\times 2}$ with $b_{ei} = \begin{bmatrix} b_{ei1} & b_{ei2} & -b_{ei3} \end{bmatrix}^T$.

3.3 Complete Averaged State-Space Model of n-Cell MLC

There are various possible state-space representations for a n–cell MLC depending on number of cells and the configuration in which they are connected inside each PC_i. Here it is assumed that each PC_i contains only one Cell_i so using (31) and (32) as basic building block, the state-space system for thermal subsystem of n cells can be written as follows:

$$\dot{X}_t = A_t X_t + \hat{G}_t(x_L)\, \hat{u} + W_t\, T_{f0}, \quad Y = C_t X_t \tag{33}$$

Here $A_t \in \mathbb{R}^{n\times n}$ is a lower triangular system matrix with coefficients a_{tij} defined by (9) and (10) , $\hat{G}_t(x_L) = \text{diag}\,(\hat{g}_{t1}(x_L), \cdots, \hat{g}_{tn}(x_L)) \in \mathbb{R}^{n\times 2n}$ is a load current-dependent input matrix for thermal subsystem, $W_t = \begin{bmatrix} b_{t1} & \cdots & b_{tn} \end{bmatrix}^T \in \mathbb{R}^n$, with coefficients b_{ti} defined by (11), is the scaling vector for the inlet fluid temperature and $C_t = I_n \in \mathbb{R}^{n\times n}$ is an output matrix, $X_t = \begin{bmatrix} X_{t1} & \cdots & X_{tn} \end{bmatrix}^T \in \mathbb{R}^n$ is a thermal state vector, $\hat{u} = \begin{bmatrix} \hat{u}^T_1 & \cdots & \hat{u}^T_n \end{bmatrix}^T \in \mathbb{R}^{2n}$ is the input vector, $T_{f0} \in \mathbb{R}$ is the known fluid temperature at the inlet and $Y \in \mathbb{R}^n$ is an output vector. Similarly the electrical subsystem of n–cells is given by:

$$\dot{X}_e = A_e X_e + \hat{G}_e(x_L)\, \hat{u} \tag{34}$$

Here $A_e = \text{diag}\,(A_{e1}, \cdots, A_{en}) \in \mathbb{R}^{3n\times 3n}$ is a system matrix and $\hat{G}_e(x_L) = \text{diag}\,(\hat{g}_{e1}(x_L), \cdots, \hat{g}_{en}(x_L)) \in \mathbb{R}^{3n\times 2n}$ is a load current-dependent input matrix for electrical subsystem, $X_e = \begin{bmatrix} X^T_{e1} & \cdots & X^T_{en} \end{bmatrix}^T \in \mathbb{R}^{3n}$ is an electrical state vector, $\hat{u} \in \mathbb{R}^{2n}$ is the input vector. Now the two subsystems can be combined in diagonal form:

$$\underbrace{\begin{bmatrix} \dot{X}_t \\ \dot{X}_e \end{bmatrix}}_{\dot{X}} = \underbrace{\begin{bmatrix} A_t & 0 \\ 0 & A_e \end{bmatrix}}_{A} \underbrace{\begin{bmatrix} X_t \\ X_e \end{bmatrix}}_{X} + \underbrace{\begin{bmatrix} \hat{G}_t(x_L) \\ \hat{G}_e(x_L) \end{bmatrix}}_{\hat{G}(x_L)} \hat{u} + \underbrace{\begin{bmatrix} W_t \\ 0 \end{bmatrix}}_{W} T_{f0}$$

$$\dot{X} = AX + \hat{G}(x_L)\hat{u} + W T_{f0}, \quad Y = CX \tag{35}$$

Where $A \in \mathbb{R}^{4n\times 4n}$ is a system matrix, $\hat{G}(x_L) \in \mathbb{R}^{4n\times 2n}$ is a load current-dependent input matrix for complete system, $C = \begin{bmatrix} C_t & 0 \end{bmatrix} \in \mathbb{R}^{n\times 4n}$ is the output matrix. $X \in \mathbb{R}^{4n}$ is a state vector, $\hat{u} \in \mathbb{R}^{2n}$ is the input vector and $W \in \mathbb{R}^{4n}$ is the scaling vector for the inlet fluid temperature.

4. OPTIMIZATION PROBLEM

In this section, the optimization problem is formulated for `OP` scheme to achieve cell balancing in terms of both temperature and SoC. The averaged state-space model derived in previous section is used along with an objective function and some constraints as described below.

4.1 Definition of Objective Function

The objective is to equalize the SoC of all cells at the final time and keep both the SoC and temperature deviations among the cells within a certain zone during the whole drive cycle. These objectives will be specified as constraints in the next subsection. In addition to this, the aim is to minimize the temperature deviations among battery cells which is specified here as the following objective function:

$$J(Y) = \int_0^{t_f} (Y_1 - Y_2)^2 + \cdots + (Y_{n-1} - Y_n)^2 dt \tag{36}$$

To bring $J(Y)$ on the quadratic form in X, let's define $Q = C^T \bar{Q}_1 \bar{Q}^T_1 C$ with $\bar{Q}_1 = \text{diag}\,(q_1, \cdots, q_{n-1}) \in \mathbb{R}^{n\times(n-1)}$ where $q_i = \begin{bmatrix} 1 & -1 \end{bmatrix}^T$. Now the objective function (36) can be rewritten on the following standard quadratic form:

$$J(X) = \int_0^{t_f} X^T Q X dt \tag{37}$$

4.2 Definition of Constraints

During run-time we want SoC of all cells to stay within a certain zone from each other given by:

$$-\Delta SoC \le (X_{ei3}(t) - X_{ej3}(t)) \le \Delta SoC, \quad \forall t, \forall i,\, j \in \{1, 2, \cdots, n\} \tag{38}$$

and at final time the SoC of all cells should be equal:

$$X_{ei3}(t_f) = X_{ej3}(t_f) \quad \forall i,\, j \in \{1, 2, \cdots, n\} \tag{39}$$

Also the SoC of each Cell_i must stay within following zone:

$$0 \le X_{ei3}(t) \le 1 \quad \forall t, \forall i \in \{1, 2, \cdots, n\} \tag{40}$$

To ensure tight thermal balancing, in addition to minimizing the deviations of cell temperatures, there is a hard

constraint to keep temperature deviations among the cells in the following zone:

$$-\Delta T_s \leq (T_{si}(t) - T_{sj}(t)) \leq \Delta T_s \quad \forall t, \forall i, j \in \{1, \cdots, n\} \tag{41}$$

Moreover, there is the safety constraint on the maximum operating temperature of each cell:

$$T_{si}(t) \leq T_{\text{smax}} \quad \forall t, \forall i \in \{1, 2, \cdots, n\} \tag{42}$$

where T_{smax} is the maximum operating temperature allowed for each Cell_i. The objective to track demanded load voltage (v_{Ld}) can be written as the following constraint:

$$v_{Ld} = \sum_{i=1}^{n} \left[(f(X_{ei3}) - X_{ei1} - X_{ei2})\, u_i - b_{ri} |u_i|\, x_L \right] \tag{43}$$

The v_{Ld} is normally provided by the higher supervisory block called Energy Management System (EMS) in context of Hybrid Electric Vehicles (HEV). The $u_i = [1 \ -1]\, \hat{u}_i$ is the duty cycle of Cell_i. In this study it is assumed that $f(X_{ei3})$ is constant and X_{ei1} and X_{ei2} are negligible which is a normal assumption used for developing the EMS for (P)HEVs, see Guzzella and Sciarretta (2005). These assumptions are being made to preserve the convexity of the problem. There is a constraint on the maximum current as well that each battery cell can supply:

$$x_L\, u_i \in [\bar{i}_{Bimin}, \bar{i}_{Bimax}] \tag{44}$$

where $\bar{i}_{Bimin}$ and $\bar{i}_{Bimax}$ are, respectively, minimum and maximum battery current limits. There are some constraints on the control signal $\hat{u}_i = [u_{i1} \ u_{i2}]^T \in \mathbb{R}^2$ given by:

$$\begin{aligned} &u_{i1} \in [0, 1], \quad u_{i2} \in [0, 1], \quad |u_i| = (u_{i1} + u_{i2}) \in [0\,, 1], \\ &\text{and} \quad u_i = (u_{i1} - u_{i2}) \in [-1\,, 1] \end{aligned} \tag{45}$$

As per the definition of u_{i1} and u_{i2} given in previous section, they cannot be nonzero simultaneously due to shoot-through problem so to ensure the safety, the following constraint is imposed:

$$u_{i1}\, u_{i2} = 0 \tag{46}$$

Note that the last constraint is non-convex and we need to get rid of it in order to preserve convexity of the problem.

4.3 Definition of Optimization Problem

Now we can write an optimization problem as follows:

$$J^0 = \min_{\hat{u}} \int_0^{t_f} X^T Q X \mathrm{d}t \quad \text{subject to}$$

$$\begin{cases} \dot{X} = AX + \hat{G}(x_L)\hat{u} + W\, T_{f0}, \\ \text{Constraints} \ \ (38) - (46), \\ x_L(t) \ \ \text{and} \ \ T_{f0} \ \ \text{are known.} \end{cases} \tag{P-I}$$

The optimization problem (P-I) is non-convex due to non-convex constraint $u_{i1}\, u_{i2} = 0$. In the next subsection, some assumptions are made to restore the convexity and simplify the problem.

4.4 Solution of Optimization Problem Using `CVX`

To solve problem (P-I) we used `CVX`, a MATLAB-based package for specifying and solving convex programs, see Grant and Boyd (2011), Grant and Boyd (2008), using disciplined convex programming ruleset, see Boyd and Vandenberghe (2006). Before setting up the optimization problem (P-I) in `CVX`, the non-convex constraint ($u_{i1}\, u_{i2} = 0$) need to be removed. In this study, the cell balancing is achieved by assuming that modes of all PCs belong *either* to the set {Mode–1 , Mode–3} *or* {Mode–2 , Mode–3} *but not* to {Mode–1 , Mode–2} at any time instant. In other words, it is not allowed at any time instant to charge any cell while discharging others. Thus, using this assumption, the sign of u_i can be pre-decided based on the sign of known demanded load voltage (v_{Ld}). Therefore, if $v_{Ld} \geq 0$ then $u_{i2} = 0$ and hence $u_i = (u_{i1} - u_{i2}) \geq 0$ otherwise $u_{i1} = 0$ and consequently $u_i \leq 0$. Thus, the non-convex constraint ($u_{i1}\, u_{i2} = 0$) need not to be specified. The system has been discretized using Euler's approximation with sampling time $h = 1\,\text{sec}$. The simulation parameters are shown in table 2 where $\bar{R}_s$ is the nominal value of series resistance, R_{si}, of any Cell_i and N is the prediction (or driving) horizon in discrete time.

Table 2. Simulation Parameters

Parameters	Value	Parameters	Value
n	5	$\bar{i}_{Bimin}$	$-200\,A, \forall i$
t_f	$12\,min$	$\bar{i}_{Bimax}$	$200\,A, \forall i$
h	$1\,sec$	ΔT_s	$2^\circ C$
N	$t_f/h = 720$	ΔSoC	0.1
R_{s5}	$\bar{R}_s$ to $2.0\bar{R}_s$	T_{smax}	$40^\circ C$
$\bar{R}_s$	$6.2770\,m\Omega$	T_{f0}	$20^\circ C$
		$T_{si}(0)$	$25^\circ C, \forall i$

5. SIMULATION RESULTS

Before presenting the simulation results, we introduce some new variables which can be illustrated in plots with more clarity. Let us define the average duty cycle $\bar{u}_i = \frac{1}{N}\sum_{k=0}^{N} u_i(k)$ of Cell_i and the average temperature $\bar{X}_{ti} = \frac{1}{N}\sum_{k=0}^{N} X_{ti}(k)$ of each Cell_i over the whole driving horizon N and similarly the average temperature of the battery submodule given by $\bar{X}_{tb} = \frac{1}{n}\sum_{i=0}^{n} \bar{X}_{ti}$. Similarly the minimum and maximum temperatures in the `BSM` over the whole driving horizon are, respectively, given by:

$$X_{tmin} = \min_{\substack{i=1,\cdots,n \\ k=1,\cdots,N}} X_{ti}(k), \quad X_{tmax} = \max_{\substack{i=1,\cdots,n \\ k=1,\cdots,N}} X_{ti}(k) \tag{47}$$

To differentiate between signals of `OP` and `UDCO` the corresponding 'o' and 'u' superscripts will be used. Now we are ready to present two simulation results here.

5.1 Battery States as function of time

Here it is assumed that the last cell in downstream has almost 50% higher series resistance due to aging or some other effect. The temperature (X_{ti}), SoC (ξ_i) and the average duty cycle ($\bar{u}_i$) are plotted for each cell. Simulation results are shown in Figure 5 for both `OP` and `UDCO` . Figure 5(a) shows the drive cycle data i.e. demanded power, voltage and current profiles. Figure 5(b) shows temperatures of all cells for `OP` and Figure 5(c) for `UDCO` policy. It is clearly seen that temperature of Cell_5 using `UDCO` policy is significantly higher compared to that of `OP` . Moreover `OP` has achieved good thermal balancing while keeping temperatures of all cells within $\pm 2^\circ$C zone. Figure 5(d) shows the SoC of all cells using `OP` scheme and as shown it has simultaneously achieved very good

balancing in SoC as well. The SoC for `UDCO` scheme is not shown here but it is quite intuitive i.e. uniformly decays for each cell. Figure 5(e) shows $\bar{u}_i(t)$ for each cell. The horizontal dashed black line shows the average duty $\bar{u}_i^u$ of each cell for `UDCO` policy and colored vertical bars shows the average duty $\bar{u}_i^o$ of each cell for `OP` scheme. The internal resistance R_{s5} of Cell_5 is almost 50% higher than other cells and Cell_5 is the most downstream cell too. Thus, as shown in Figure 5(e), the naturally optimal policy is to use Cell_5 less compared to others and Cell_1, which is in the best thermal condition, should be used most.

5.2 Battery Average Temperatures Versus R_{s5}

Figures 5(f) and 5(g) respectively show the variation in temperature of a battery submodule (`BSM`) and that of each cell versus increase in resistance of Cell_5. It is clearly seen in Figure 5(f) that the maximum temperature (X_{tmax}) in the `BSM` when using the `UDCO` policy is significantly higher compared to that of `OP` . Similarly, as shown in Figure 5(g), the average temperature ($\bar{X}_{t5}$) of Cell_5 suffers from thermal run away when `UDCO` policy is used, whereas the temperature of all cells remains well balanced if `OP` policy is used instead. Therefore, in the absence of the `OP` scheme, Cell_5 faces higher thermal stresses and may fail before others and hence may reduce the life of whole battery submodule.

6. CONCLUSION AND FUTURE WORK

This article has investigated the potential benefit of optimally using the extra DoF of MLC for simultaneous balancing of both SoC and temperature of cells. The complete state-space electro-thermal model has been derived and a constrained convex optimization problem has been formulated and solved. The simulation results show that even for 50% increase in internal resistance of the downstream cell the `OP` policy, that optimally uses the extra DoF of MLC, gives significant reduction in temperature deviation among cells compared to ad hoc uniform duty cycle operation. Thus, this study encourages to investigate further to reduce computational complexity in order to implement an online version of the optimal policies.

7. ACKNOWLEDGMENTS

The authors would like to thank Nikolce Murgovski, Oskar Josefsson, Torbjörn Thiringer and Anders Grauers for all the positive discussions while developing this work.

REFERENCES

Bentley, W. (1997). Cell balancing considerations for lithium-ion battery systems. In *Battery Conference on Applications and Advances, 1997., 12th Annual*, 223 – 226.

Boyd, S. and Vandenberghe, L. (2006). *Convex Optimization*. Cambridge University Press.

Cao, J., Schofield, N., and Emadi, A. (2008). Battery balancing methods: A comprehensive review. In *Vehicle Power and Propulsion Conference, 2008. VPPC '08. IEEE*, 1 –6.

Chen, M. and Rincon-Mora, G. (2006). Accurate electrical battery model capable of predicting runtime and i-v performance. *Energy Conversion, IEEE Transactions on*, 21(2), 504 – 511.

Codeca, F., Savaresi, S., and Rizzoni, G. (2008). On battery state of charge estimation: A new mixed algorithm. In *Control Applications, 2008. CCA 2008. IEEE International Conference on*, 102 –107.

Grant, M. and Boyd, S. (2008). Graph implementations for nonsmooth convex programs. In V. Blondel, S. Boyd, and H. Kimura (eds.), *Recent Advances in Learning and Control*, Lecture Notes in Control and Information Sciences, 95–110. Springer-Verlag Limited. `http://stanford.edu/~boyd/graph_dcp.html`.

Grant, M. and Boyd, S. (2011). CVX: Matlab software for disciplined convex programming, version 1.21. `../../cvx`.

Guzzella, L. and Sciarretta, A. (2005). *Vehicle Propulsion Systems*. Springer.

He, H., Xiong, R., Zhang, X., Sun, F., and Fan, J. (2011). State-of-charge estimation of the lithium-ion battery using an adaptive extended kalman filter based on an improved thevenin model. *Vehicular Technology, IEEE Transactions on*, 60(4), 1461 –1469.

Josefsson, O., Lindskog, A., Lundmark, S., and Thiringer, T. (2010). Assessment of a multilevel converter for a phev charge and traction application. In *Electrical Machines (ICEM), 2010 XIX International Conference on*, 1 –6.

Kassakian, J., Schlecht, M., and Verghese, G. (1991). *Principles of Power Electronics*. Addison-Wesley.

Khalil, H. (2002). *Nonlinear systems*. Prentice Hall, NJ.

Krein, P. (2007). Battery management for maximum performance in plug-in electric and hybrid vehicles. In *Vehicle Power and Propulsion Conference, 2007. VPPC 2007. IEEE*, 2 –5.

Kuhn, B., Pitel, G., and Krein, P. (2005). Electrical properties and equalization of lithium-ion cells in automotive applications. In *Vehicle Power and Propulsion, 2005 IEEE Conference*, 5 pp.

Lee, W.C., Drury, D., and Mellor, P. (2011). Comparison of passive cell balancing and active cell balancing for automotive batteries. In *Vehicle Power and Propulsion Conference (VPPC), 2011 IEEE*, 1 –7.

Lukic, S., Cao, J., Bansal, R., Rodriguez, F., and Emadi, A. (2008). Energy storage systems for automotive applications. *Industrial Electronics, IEEE Transactions on*, 55(6), 2258 –2267.

Mahamud, R. and Park, C. (2011). Reciprocating air flow for li-ion battery thermal management to improve temperature uniformity. *Journal of Power Sources*, 196(13), 5685 – 5696.

Malinowski, M., Gopakumar, K., Rodriguez, J., and Pe andrez, M. (2010). A survey on cascaded multilevel inverters. *Industrial Electronics, IEEE Transactions on*, 57(7), 2197 –2206.

Mohan, N., Undeland, T.M., and Robbins, W.P. (2003). *Power Electronics: Converters, Applications, and Design*. John Wiley & Sons; 2003, 3 edition.

Motloch, C., Christophersen, J., Belt, J., Wright, R., Hunt, G., Tartamella, T., Haskins, H., and Miller, T. (2002). High-Power Battery Testing Procedures and Analytical Methodologies for HEV's. *SAE 2002-01-1950*.

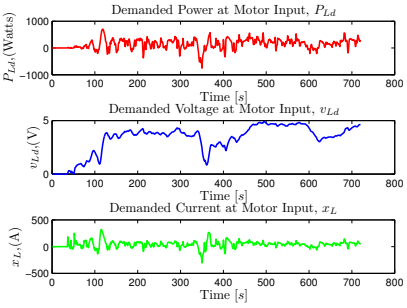

(a) Drive Cycle: Demanded Power, Voltage and Current Profile.

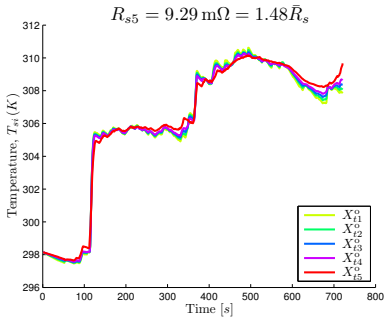

(b) Optimal Temperature of each cell for OP . Despite R_{s5} being 50% higher, OP has successfully achieved thermal balancing among all cells.

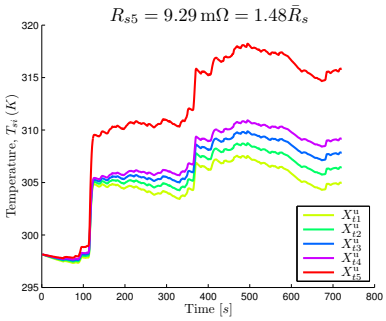

(c) Temperature of each cell for UDCO . Red: *Hottest Cell*, Light Green: *Coldest Cell*. Cell_5 suffers from thermal run away as shown in red.

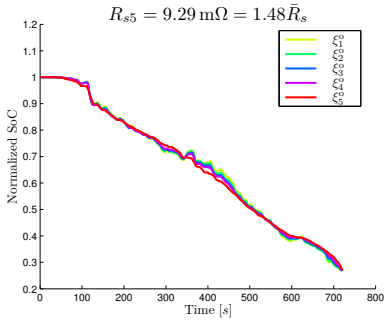

(d) Optimal SoC of each cell for OP . The plot shows that OP has simultaneously achieved the SoC balancing in addition to thermal balancing shown in Fig. 5(b).

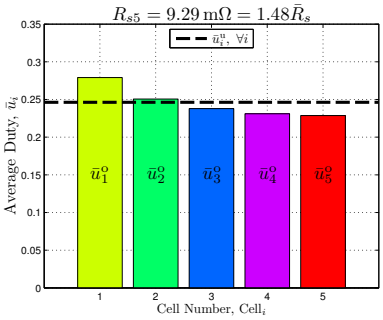

(e) Optimal average duty cycles $\bar{u}_i^o$ of each Cell_i computed by OP . The dashed horizontal black line shows the uniform average duty cycle computed by UDCO .

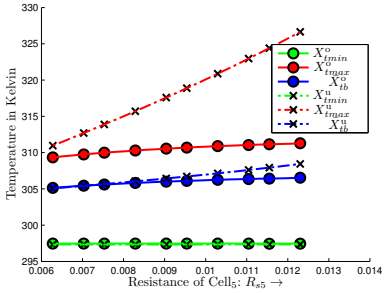

(f) Minimum, Maximum and Average Temperature of BSM as function of R_{s5} for both OP and UDCO .

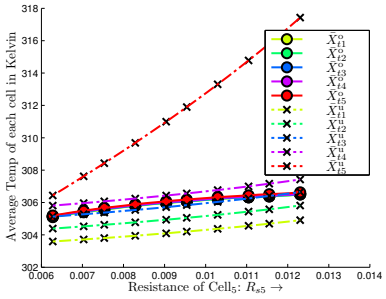

(g) Variation in $\bar{X}_{ti}$ of all cells as a function of R_{s5} for both OP and UDCO .

Fig. 5. Simulation results and comparison between OP and UDCO . The plots show that despite the resistance (R_{s5}) of the most down stream Cell_5 being 50% higher compared to other cells, OP has still successfully achieved simultaneous thermal and SoC balancing among all cells whereas uniform use of cells is naturally not optimal in this situation.

Park, C. and Jaura, A. (2002). Transient heat transfer of 42 V Ni-MH batteries for an HEV application. *Future Car Congress*.

Park, C. and Jaura, A. (2003a). Dynamic thermal model of Li-Ion battery for predictive behavior in hybrid and fuel cell vehicles. *SAE transactions*, 112(3), 1835–1842.

Park, C. and Jaura, A. (2003b). Reciprocating battery cooling for hybrid and fuel cell vehicles. *ASME International Mechanical Engineering Congress and Exposition (IMECE2003), Washington, DC, USA*, 425–430.

Pesaran, A. and Vlahinos, A, B.S. (1997). Thermal performance of EV and HEV battery modules and packs. *Proceedings of the 14th International Electric Vehicle Symposium, Orlando, Florida*.

Rodriguez, J., Franquelo, L., Kouro, S., Leon, J., Portillo, R., Prats, M., and Perez, M. (2009). Multilevel converters: An enabling technology for high-power applications. *Proceedings of the IEEE*, 97(11), 1786 –1817.

Sirisukprasert, S. (2004). *The Modeling and Control of a Cascaded-Multilevel Converter-Based STATCOM*. PhD Thesis, Virginia Tech.

Smith, K., Markel, T., Gi-Heon, K., and Pesaran, A. (2010). Design of electric drive vehicle batteries for long life and low cost. *Accelerated Stress Testing and Reliability (ASTR), IEE Workshop on*.

Tolbert, L., Peng, F.Z., and Habetler, T. (1999). Multilevel converters for large electric drives. *Industry Applications, IEEE Transactions on*, 35(1), 36 –44.